

# Melt Processing of Semicrystalline E/EP/E Triblock Copolymers near the Order–Disorder Transition

Peter Kofinas and Robert E. Cohen\*

Department of Chemical Engineering, Massachusetts Institute of Technology,  
77 Massachusetts Avenue, Cambridge, Massachusetts 02139

Received May 31, 1994; Revised Manuscript Received August 30, 1994®

**ABSTRACT:** A series of semicrystalline triblock copolymers E/EP/E, of poly(ethylene) (E) and poly(ethylenepropylene) (EP) were subjected to high levels of plane strain compression using a channel die. The processing was carried out at 150 °C, a temperature which lies well above both the E block melting points (99–103 °C) and the quiescent order–disorder transitions (ca. 106 °C) for these samples. The lamellar orientation relative to the specimen boundaries was determined using two dimensional small-angle X-ray scattering. By using a 2.4 MPa applied stress on the channel die, the lamellae orient parallel to the plane of shear, while processing at an applied stress of 8.0 MPa causes the lamellae to orient perpendicular to the plane of shear. Gas permeability coefficients  $P$  for He and CO<sub>2</sub> were measured at 25 °C for E/EP/E 25/50/25 specimens and compared to modeling predictions. The upper bound (lamellae aligned in parallel with respect to the permeation direction) and lower bound (series lamellar alignment) models were compared to experimental permeation data on the corresponding oriented triblock specimens.

## 1. Introduction

Melt processing of block copolymers presents certain obstacles and opportunities to the user. It is necessary to know whether or not the melt is homogeneous or heterogeneous, i.e., the position of the order–disorder temperature,  $T_{ODT}$ , relative to the selected processing temperature, so that the corresponding thermorheologically simple<sup>1</sup> or complex<sup>2,3</sup> behavior can be anticipated. Also of importance is the sensitivity of the order–disorder temperature to changes in process variables such as applied stress or shear rate.<sup>4,5</sup> Finally, it is becoming increasingly apparent that processing a single block copolymer material near  $T_{ODT}$  can lead to a variety of morphologies in the final product depending upon the process conditions employed.<sup>6–9</sup>

In this context, the behavior of a block copolymer with at least one crystallizable moiety is particularly interesting because of the multiplicity of “frozen-in” morphologies which can be expected.<sup>11,12</sup> In the present paper we demonstrate this process-dependent morphological control for a series of triblock copolymers comprised of poly(ethylene)/poly(ethylenepropylene)/poly(ethylene) (E/EP/E). We also provide quantitative information on the length scale of the lamellar periodicity exhibited by the copolymers at room temperature. To demonstrate the principle that these process-induced morphologies can have a profound influence on properties of block copolymers, we have measured<sup>12,13</sup> the gas permeability of our oriented specimens and have compared the results to the behavior of random (spherulitic) specimens crystallized from quiescent melts.

## 2. Experimental Section

The E/EP/E triblock copolymers were synthesized by hydrogenation of 1,4-poly(butadiene)/1,4-poly(isoprene)/1,4-poly(butadiene) triblock copolymers. The butadiene block consists of 10% 1,2, 35% trans 1,4, and 55% cis 1,4 PB, while isoprene block contains 93% cis 1,4 and 7% 3,4 PI. The catalytic

**Table 1. Characterization of E/EP/E Specimens ( $M \times 10^{-3}$  g/mol)**

triblocks
E/EP/E 15/70/15
E/EP/E 20/60/20
E/EP/E 25/50/25
E/EP/E 30/40/30
E/EP/E 35/30/35

hydrogenation procedure<sup>14</sup> has been used extensively in this laboratory.<sup>15,16</sup> Hydrogenated PB thus resembles low-density poly(ethylene) (E) and hydrogenated PI is essentially perfectly alternating ethylene propylene rubber (EP). The molecular weights of each block for the E/EP/E triblocks are listed in Table 1. These values were determined from GPC measurements on the polydiene precursors, from knowledge of reactor stoichiometry and conversion, and from a previous demonstration<sup>14</sup> that little or no degradation occurs during the hydrogenation reactions. The melting points of the crystallizable E blocks for the series of E/EP/E copolymers, were all between 99 and 103 °C, as determined by a DSC instrument at a heating rate of 10 °C/min.

Rheological measurements were performed on a Rheometrics Dynamic Spectrometer Model RDS-II operated in the dynamic mode ( $\omega = 0.1$  rad/s) with a parallel plate fixture. Dynamic shear moduli measurements were conducted using a 0.5% strain amplitude. The sample temperature was controlled between 70 and 150 °C using a thermally regulated nitrogen purge. The order–disorder transition temperature was determined by measuring  $G'$  at a fixed frequency of 0.1 rad/s while slowly heating (0.2 °C/min) or cooling the specimens.

A channel die, the description of which is given in detail elsewhere,<sup>17–20</sup> was used to subject the polymers to plane strain compression up to compression ratios of 12. Figure 1 shows a sketch of the channel die and defines the three principal directions, i.e., the lateral constraint direction (CD), the free (or flow) direction (FD), and the loading direction (LD). The temperature of the channel die was always maintained at 150 °C during the compression flow, and the selected load was maintained until the desired compression ratio was achieved. The compressed specimens were quenched under load to room temperature, followed by load release. The final compression ratio was determined from the reduction of the thickness of the samples.

The change in lamellar orientation due to deformation was studied by means of small-angle X-ray scattering (SAXS). The SAXS measurements were performed on a computer-controlled

\* Author to whom all correspondence should be directed.

© 1995 American Chemical Society

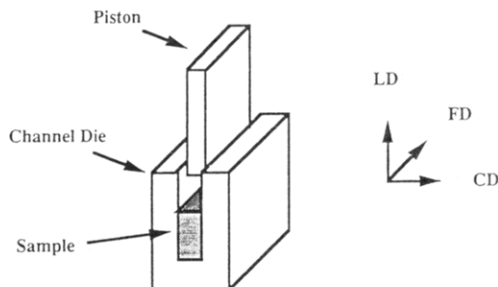


Figure 1. Channel die apparatus.

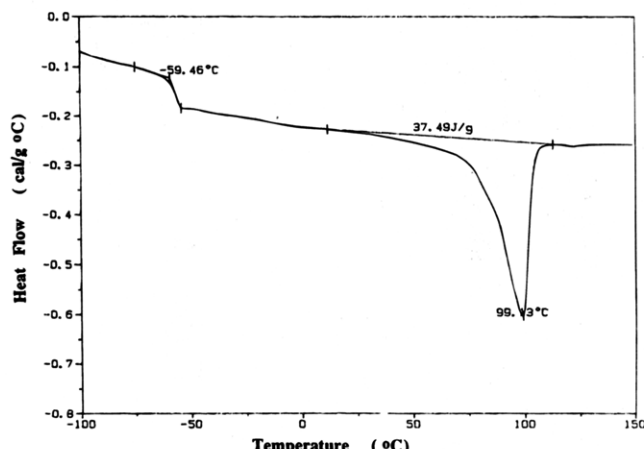


Figure 2. DSC scan for E/EP/E 25/50/25.

system consisting of a Nicolet two-dimensional position-sensitive detector associated with a Rigaku rotating-anode generator operating at 40 kV and 20 mA and providing Cu K $\alpha$  radiation. The primary beam was collimated by two Ni mirrors. In this way the X-ray beam could be effectively focused onto a small beam stop (2 mm diameter) without losing much intensity. The specimen to detector distance was 2.7 m, and the scattered beam path between the specimen and the detector was enclosed by an aluminum tube filled with helium gas in order to minimize the background scattering.

Oriented E/EP/E specimens were prepared using channel die compression as mentioned above and discussed in greater detail below. E/EP/E spherulitic films for permeation measurements were prepared by compression molding at 190 °C by means of a hydraulic press. Prior to permeation measurements, these compression molded films were annealed under vacuum at 120 °C for two days and then cooled slowly to room temperature. The gases used in this study, He and CO<sub>2</sub>, had purities in excess of 99.99%. Gas permeability coefficients ( $P$ ) were determined from steady-state measurements using a variable-volume permeation apparatus.<sup>21</sup> All measurements were carried out at 25 °C with a pressure difference of 10.5 psig across the sample films.

### 3. Results

A DSC spectrum of the E/EP/E 25/50/25 triblock is shown in Figure 2. The peak centered at 99 °C defines the nominal melting point of poly(ethylene) in this sample. The large breadth of the melting curve indicates the presence of a wide distribution of crystal sizes and perfection. Crystallization occurs almost instantaneously as the polymers are cooled below their melting point; varying the thermal history has little observable effect on the degree of crystallinity. Using polarized light microscopy we observed that all triblocks, prior to channel die processing, exhibit spherulitic morphology when crystallized from the melt, even in the case of samples containing as little as 30% poly(ethylene). These observations suggest that a lamellar morphology predominates over the entire composition range exam-

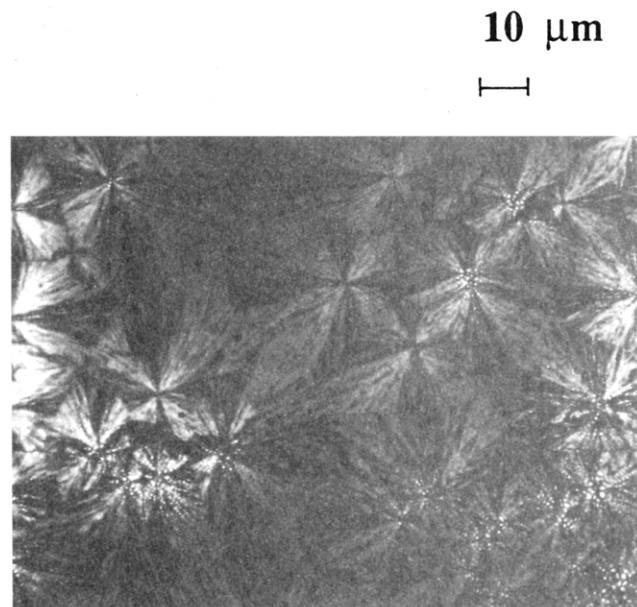
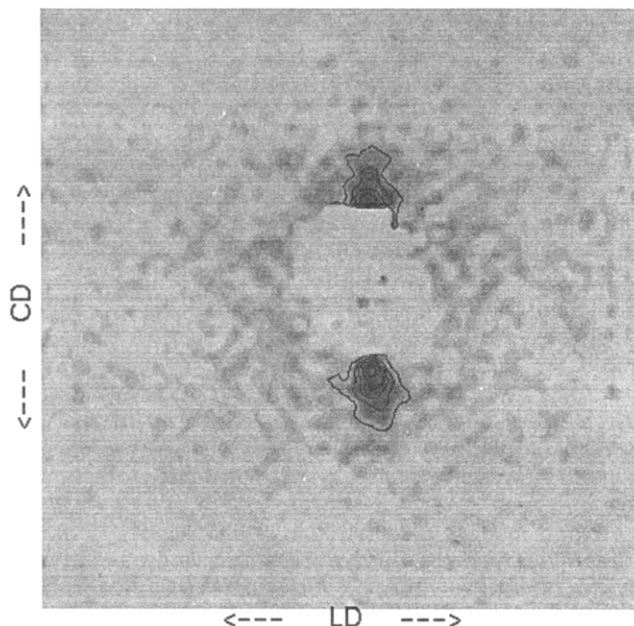
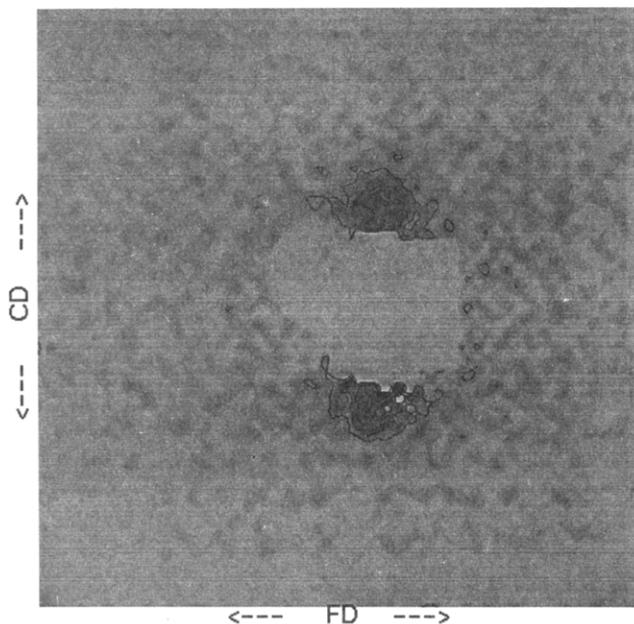


Figure 3. Optical micrograph E/EP/E 25/50/25 crystallized from the melt.

ined here. A representative micrograph of the spherulitic morphology of the E/EP/E polymers is shown in Figure 3.

The 2D SAXS patterns of the E/EP/E 15/70/15 and 25/50/25 specimens, subjected to plane strain compression at 150 °C and then quenched to room temperature, are shown in Figures 4 and 5. These channel die experiments were conducted at compression ratios of  $\lambda = 4$  to  $\lambda = 12$ , and an applied stress  $\sigma = 8.0$  MPa. The SAXS patterns are shown in the form of contour plots. A linear gray-scale colormap is used to represent intensity contours ranging from 5% to 90% of total intensity, with darker regions representing higher intensities. For these specimens there is no significant scattering when the X-ray beam is parallel to the constraint direction; spread-out spots on the 2D detector are observed when the sample is irradiated along the flow and loading directions. The degree of alignment under shear deformation of the semicrystalline lamellar microdomains decreases with increasing amorphous content, as evidenced by the spreading out of the oriented SAXS patterns both in the loading (compare Figures 4a and 5a) and flow (Figures 4b and 5b) directions.

The same E/EP/E 25/50/25, when processed at 150 °C (Figure 6) but at an applied stress of  $\sigma = 2.4$  MPa, shows a set of SAXS patterns which are completely different from the results (Figure 5) obtained at the higher applied stress  $\sigma = 8.0$  MPa. The view from the loading direction reveals no scattering and broad spots are obtained when the X-ray beam is parallel to either the constraint direction or to the flow direction. The SAXS patterns thus reveal that the morphology changes from lamellae oriented perpendicular to the plane of shear,<sup>6-8</sup> when the specimen is deformed at high applied stress (8.0 MPa), to lamellae oriented parallel to the shear plane for samples processed at low applied stress (2.4 MPa). The results for the lamellar orientations in the textured E/EP/E triblocks as deduced from the SAXS analysis, are summarized schematically in Figure 7. Table 2 summarizes the lamellar spacings observed from the SAXS patterns for these spherulitic triblocks along with the values obtained for the oriented morphologies for the same set of materials. Error bars of



**Figure 4.** SAXS of E/EP/E 15/70/15 oriented above the E block melting point via plane strain compression ( $\lambda = 4$  to  $\lambda = 12$ ,  $\sigma = 8.0$  MPa): (a, top) X-ray beam in the loading direction; (b, bottom) X-ray beam in the flow direction. The third corresponding figure for the case in which the X-ray beam is in the constraint direction shows no significant scattering pattern.

10–15% are associated with the lamellar spacings.

The behavior of the E/EP/E 25/50/25 triblock in the melt was further investigated by performing high-temperature SAXS experiments: Specimens were prepared using an applied stress of  $\sigma = 8.0$  MPa at 150 °C, so that the orientation produced would be lamellae perpendicular to the plane of shear (Figure 8a). The samples were then mounted in a Mettler hot stage, which was placed within the X-ray beam path. As the annealed E/EP/E 25/50/25 triblock is heated toward the 99 °C melting point, the SAXS pattern still shows the perpendicular lamellar orientation, but the intensity is reduced (see Figure 8b,  $T = 80$  °C). The contrast in the X-ray experiment arises from the significantly larger density of the semicrystalline E domains compared to the amorphous EP blocks. The crystallites in the

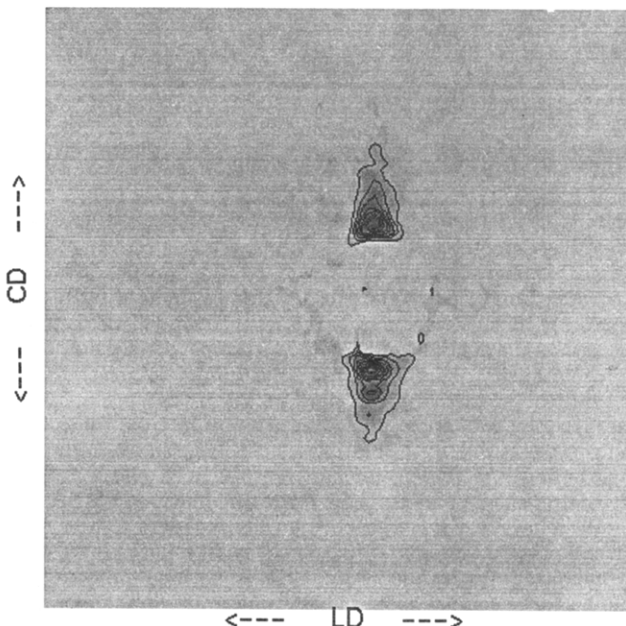
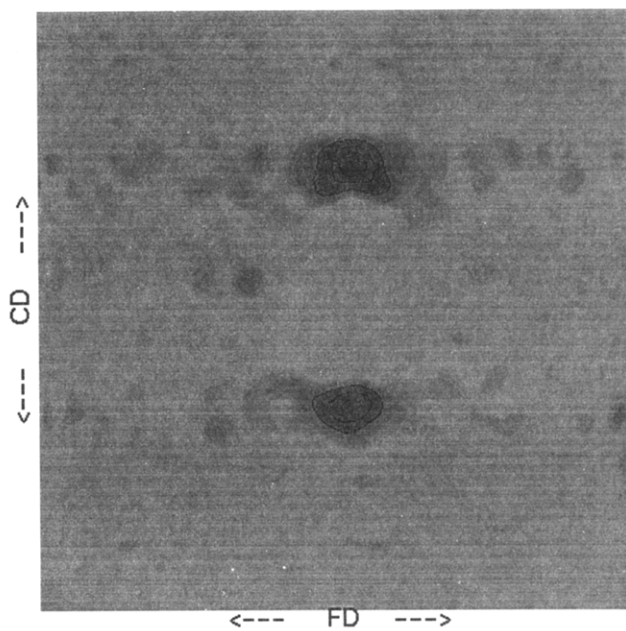


**Figure 5.** SAXS of E/EP/E 25/50/25 oriented above the E block melting point via plane strain compression ( $\lambda = 4$  to  $\lambda = 12$ ,  $\sigma = 8.0$  MPa): (a, top) X-ray beam in the loading direction; (b, bottom) X-ray beam in the flow direction. The third corresponding figure for the case in which the X-ray beam is in the constraint direction shows no significant scattering pattern.

E/EP/E triblock begin melting as the 99 °C melting point is approached, thus reducing the density mismatch and the observed SAXS intensity. No SAXS pattern can be observed at temperatures above  $T_m$  (Figure 8c). However, the absence of contrast in the SAXS pattern of the melt does not necessarily imply the existence of a homogeneous melt. To inquire into the possibility of the existence of a heterogeneous melt, the E/EP/E samples were annealed at 105 °C (Figure 8d) and at 106 °C (Figure 8e) for 24 h and then cooled back to room temperature. Samples heated up to 105 °C and annealed for a day retained their original oriented lamellar morphology which could be seen again in SAXS when the sample was cooled back to room temperature. Crystallization occurred within the oriented, microphase separated melt, and therefore the original oriented

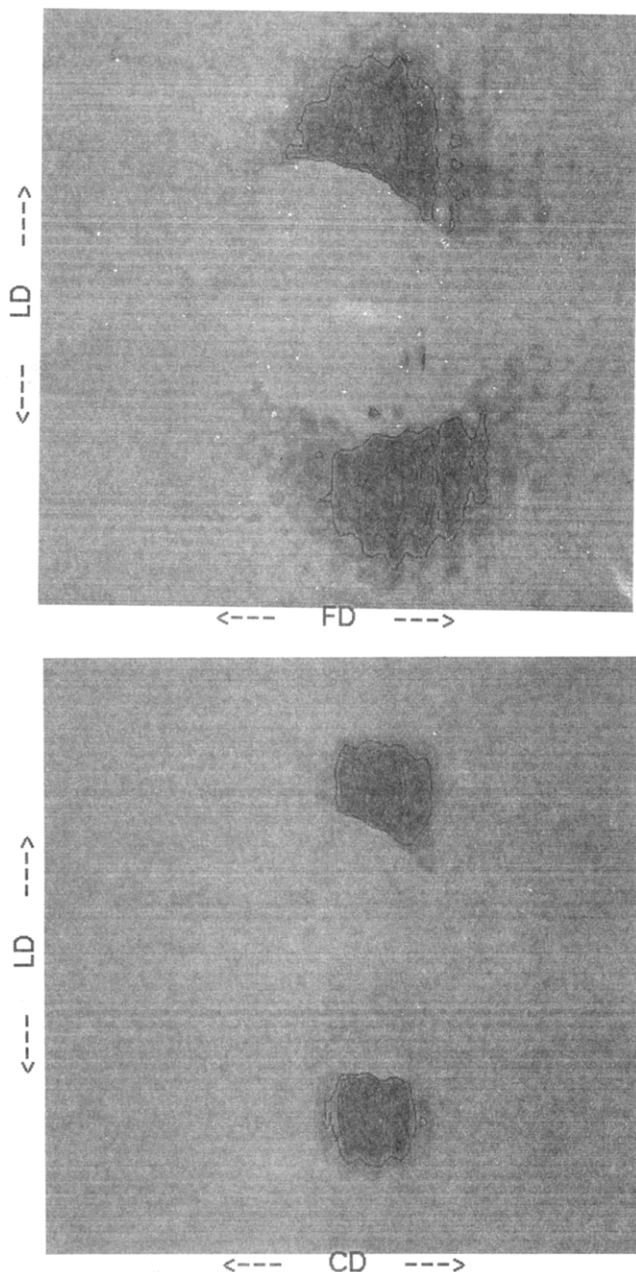


**Figure 6.** SAXS of E/EP/E 25/50/25 oriented above the E block melting point via plane strain compression ( $\lambda = 4$  to  $\lambda = 12$ ,  $\sigma = 2.4$  MPa): (a, top) X-ray beam in the constraint direction; (b, bottom) X-ray beam in the flow direction. The third corresponding figure for the case in which the X-ray beam is in the loading direction shows no significant scattering pattern.

morphology reappears at room temperature. Annealing at 105 °C might have actually improved the lamellar orientation somewhat, as evidenced by the increase in intensity of SAXS pattern after cooling back to room temperature. The ring SAXS pattern of the E/EP/E sample annealed at 106 °C the melt became homogeneous because upon subsequent cooling, crystallization produced a random spherulitic morphology similar to what is shown in the optical micrograph of Figure 3. Therefore, between 105 and 106 °C a transition occurred from an ordered to a disordered melt.

Rheological measurements on the 25/50/25 triblock showed a dramatic (3 orders of magnitude) reduction on the storage modulus in the range of the E block melting point (99 °C); a subtle but reproducible increase in slope of the plateau regime occurred at 104 °C for

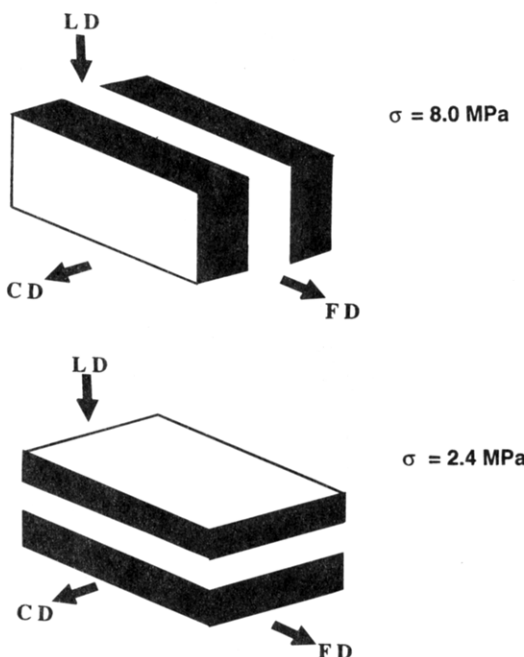


**Figure 7.** Sketch of lamellar orientations in E/EP/E specimens processed above the E block melting point

**Table 2. Lamellar Long Periods for Spherulitic and Oriented Samples**

triblocks	spherulitic	$\sigma = 8.0$ MPa	$\sigma = 2.4$ MPa
E/EP/E 15/70/15	470	410	
E/EP/E 20/60/20	480		
E/EP/E 25/50/25	500	440	490
E/EP/E 30/40/30	530	420	
E/EP/E 35/30/35	570		

this triblock copolymer.<sup>12</sup> For purposes of comparison, E/EP diblocks were examined in identical conditions. The same increase in slope was observed for an E/EP 60/40 diblock near 145 °C. The E/EP 100/100 diblock showed no transition of this type up to 200 °C, at which point noticeable degradation of the specimen occurred.<sup>12</sup>

#### 4. Discussion

**4.1. Morphology and Processing.** The channel die melt processing behavior of the E/EP systems of our previous study<sup>11</sup> and of the E/EP/E triblocks examined here can be rationalized from an examination of the position of the specimens with respect to Leibler's phase diagram<sup>22</sup> and using the results of previous studies on wholly amorphous diblock copolymers.<sup>8</sup> The block copolymers we have examined contained N<sub>C</sub> and N<sub>A</sub> units of chemically distinct segments, where C denotes crystallizable and A amorphous. At sufficiently high temperatures (or low total degree of polymerization  $N_T = N_A + N_C$ ) the melt is disordered or homogeneous, while at low temperatures (or high  $N_T$ ) various ordered structures<sup>22</sup> are observed. Equilibrium phase behavior was expressed by Leibler in terms of the polymer composition  $f$  and the reduced parameter  $\chi N_T$  (where  $\chi$  represents the Flory-Huggins segment-segment interaction parameter).

$\chi N_T$  for each of our E/EP and E/EP/E copolymer systems was calculated using values reported by Bates et al.;<sup>23</sup> the results are plotted versus the E fraction in the copolymer in the format of Leibler's phase diagram at 150 °C in Figure 9. The highest molecular weight diblocks (upper row of solid points on the phase diagram) are clearly above the order-disorder boundary

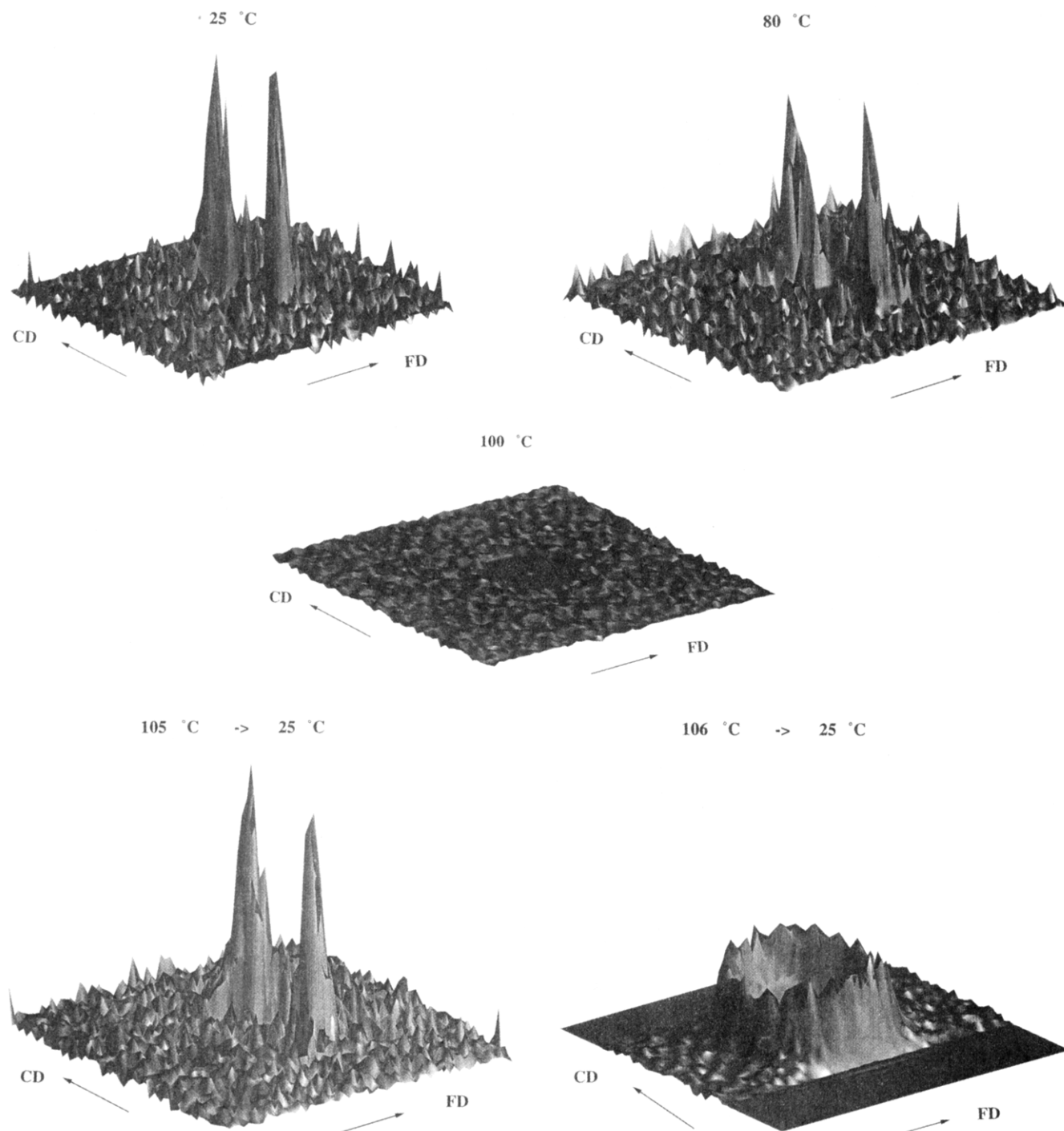


**Figure 8.** SAXS temperature study of E/EP/E 25/50/25 oriented above the E block melting point via plane strain compression,  $\sigma = 8.0$  MPa, X-ray beam in the loading direction: (a, top left) 25 °C, (b, top right) 80 °C, (c, middle center) 100 °C (melt), (d, bottom left) annealed for 24 h at 105 °C, cooled to 25 °C, (e, bottom right) annealed for 24 h at 106 °C, cooled to 25 °C.

at the selected temperature, thus indicating that at equilibrium they form heterogeneous melts; the 100 K diblocks and the triblocks, however, are close to the order-disorder transition (ODT). Figure 9 shows that when the 100 K diblocks and triblocks are processed at 150 °C in the channel die, these materials would be homogeneous if the quiescent ODT controlled the morphological behavior during processing. However, it is known<sup>5,4,7</sup> that processing parameters such as shear stress and shear rate shift the ODT to higher temperatures resulting in a downward shift of the curve in Figure 9 which could bring all diblocks and triblocks to the heterogeneous regime just above the ODT.

Cates and Milner<sup>5</sup> first investigated in a theoretical study the influence of shear fields on  $T_{ODT}$ . They showed that increasing the steady shear rate on a mesomorphic material exhibiting an isotropic to lamellar transition increases  $T_{ODT}$  and decreases  $T_{ODT} - T_S$ , where  $T_S$  is the stability limit for the isotropic state. These theoretical predictions were experimentally confirmed by Koppi et al.,<sup>7</sup> who used a dynamic shearing device in conjunction with small-angle neutron scattering (SANS) measurements to measure  $T_{ODT}$  and  $T_{ODT} - T_S$  in a symmetric poly(ethylenepropylene)/poly(ethyleneethylene) (EP/EE) diblock copolymer melt. They found that  $T_{ODT}$  increased by 5 °C from the quiescent

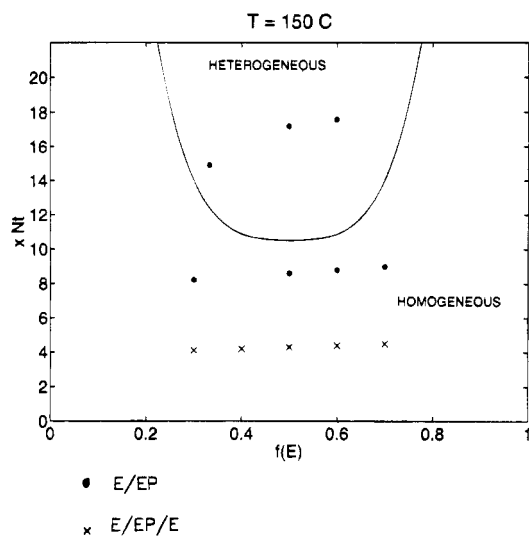


**Figure 9.** Position of the E/EP and E/EP/E copolymers relative to the order-disorder transition curve of Leibler's phase diagram at 150 °C.

EP/EE melt up to a shear rate of 10 s<sup>-1</sup>. They also managed to obtain a  $T_{ODT} - T_s$  difference of 11 °C. These studies support the conclusion from our SAXS and rheology experiments, that the E/EP and E/EP/E systems we examined form heterogeneous melts under shear.

Another related study by Almdal et al.<sup>6</sup> examined dynamically sheared EP/EE diblock copolymer melts sheared near  $T_{ODT}$ , which exhibited the parallel lamellar orientation at low shear frequencies and the perpendicular orientation at higher frequencies. At temperatures further away from the ODT, the parallel orientation was obtained at all frequencies. Low-frequency dynamic shearing corresponds to low applied stress processing for our E/EP/E channel die experiments, since the higher applied stress on the channel die, the faster the piston moves to compress the polymer sample inside the die. Similarly, high frequencies in the dynamic shearing mode correspond to high applied stresses and perpendicular lamellae morphologies to the plane of shear. The peculiar perpendicular lamellar orientation was attributed<sup>9</sup> to the disordering ('melting') of the lamellae with immediate regrowth. The thermodynamic barrier to disordering was overcome only near the ODT, thus production of perpendicular lamellae only occurs near the ODT.<sup>5,8</sup> We find the same behavior here for the case of plane strain compression of our 100 K specimens at 150 °C, where high applied stresses correspond to high shear rates or frequencies. We therefore conclude that our E/EP and E/EP/E block copolymers form ordered heterogeneous melts under the shear field imposed from the channel die, when deformed at 150 °C above the E block melting point. As the sample is cooled under load the perpendicular lamellar phase is subsequently "frozen-in" at the onset of crystallization. The crystallization therefore is required to occur in the presence of this preexisting lamellar morphology.

**4.2. Morphology and Molecular Structure.** Several theories<sup>24,25</sup> have been proposed to describe the equilibrium morphology of lamellar semicrystalline diblock copolymer systems. Whitmore and Noolandi<sup>25</sup> developed a mean-field theory for the scaling behavior of lamellar domain spacings. They modeled the amorphous blocks as flexible chains with one end fixed at the sharp amorphous-semicrystalline interface. The

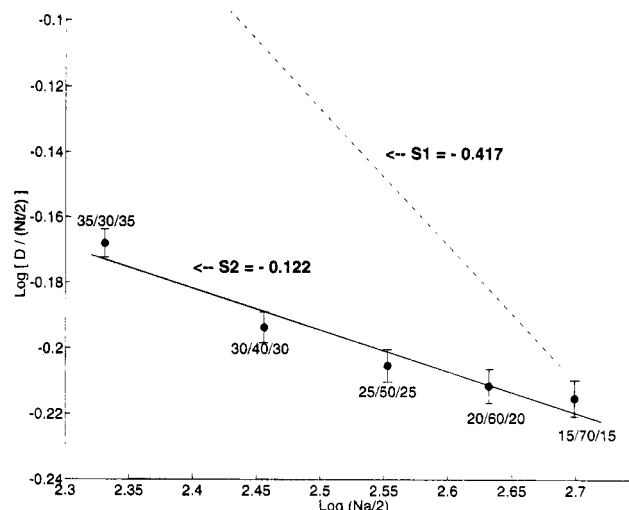


**Figure 10.** Noolandi scaling law for E/EP/E spherulitic specimens.

semicrystalline blocks were modeled as chain-folded macromolecules with one end of the chain fixed at the interface attached to a corresponding amorphous block. They performed calculations for a poly(styrene)/poly(ethylene oxide) diblock system and found  $D \approx N_T N_A^{-5/12}$  where  $N_A$  were the number of statistical segments in the amorphous block and  $N_T$  the total number of segments. Studies on the applicability of Noolandi's scaling law to other semicrystalline block copolymer systems have been carried out in this laboratory<sup>16</sup> on E/EE diblocks and elsewhere<sup>26</sup> on E/EP diblocks.

Figure 10 is a plot of the lamellar long period  $D$  versus the amorphous block length  $N_A$ . The  $D$  values were determined from the SAXS patterns of randomly oriented spherulitic E/EP/E specimens (see Table 2). The form of Figure 10 is based on the Noolandi scaling law, which requires that  $D$  becomes larger with increasing  $N_T$  while the length of the amorphous sequence,  $N_A$ , mitigates against the increasing lamellar repeat distance according to a factor  $N_A^{-5/12}$ . The theory thus predicts a straight line in Figure 10 and Noolandi's calculations lead to a slope of  $s_1 = -5/12 = -0.417$ . A calculated line of slope  $s_1$  is shown for comparison with the actual experimental data. The position of the calculated (dashed) line on the vertical axis has been arbitrarily chosen to illustrate the relationship between predicted and experimental slopes. The least-squares fit to the experimental data for the E/EP/E samples (solid line) gives a slope  $s_2 = -0.122$ . It is obvious that the scaling law does not fit perfectly to the data, but the general trend of decreasing  $D/N_T$  with increasing amorphous block length is shown clearly.

**4.3 Morphology and Gas Transport.** We have demonstrated clearly that rather dramatic morphology control is possible through changes in melt processing of block copolymers near the ODT. One set of properties which is exquisitely sensitive to such morphological change is the gas transport behavior where very simple upper and lower bound models<sup>27,28</sup> can be written for the case of permeation parallel to and perpendicular to the orientation of the lamellar structure. The intermediate case of gas permeation in a material with random lamellar orientation is also readily modeled.<sup>13,29</sup> Thus gas permeation measurements are not only useful to demonstrate the sensitivity of the material properties to processing history but also they can be used to verify the existence of the morphological features suggested

**Table 3. Permeability coefficients for E/EP/E 25/50/25 at 25 °C, 10.5 psi<sup>a</sup>**

gas	$P_{\text{ser}}^*$ (exp)	$P_{\text{ser}}^*$ (model)	$P_{\text{sph}}^*$ (exp)	$P_{\text{sph}}^*$ (model)	$P_{\text{par}}^*$ (exp)	$P_{\text{par}}^*$ (model)
He	12.2	10.9	22.5	20.5	36.2	38.3
CO <sub>2</sub>	40.8	39.0	48.3	47.5	62.4	66.1

<sup>a</sup>  $P$  in barriers. Subscript "ser" indicates series permeation; "par" indicates parallel permeation; and "sph" indicates permeation through a random spherulitic material (ref 13).

by the X-ray analyses provided above. The degree to which the limiting models describe the observed permeation data is a good reflection of the degree to which the processing has resulted in perfection of a particular lamellar arrangement.

Gas molecules are generally taken to be insoluble in polymer crystallites and, therefore, are unable to permeate through them.<sup>30</sup> Thus, gas permeation in semicrystalline polymers is essentially confined to the amorphous regions. The crystallites reduce the permeability by decreasing the volume of polymer available for penetrant solution and by constraining the transport along irregular tortuous paths between the crystallites. The reduction in permeability ( $P$ ), which is the product of the effective diffusion ( $D$ ) and solubility ( $S$ ) coefficients, will thus be proportional to the volume fraction of the crystalline phase<sup>31</sup> when all samples have a random misoriented morphology. The effect of microphase orientation on gas permeability is significant. Permeability coefficients for a film whose microdomains oriented normal to the film surface are much larger than for a film whose lamellar domains are in the same plane as the film surface.<sup>12</sup>

In a previous investigation on E/EP diblock copolymer systems<sup>13</sup> we presented a simple model of gas permeation in misoriented lamellar materials which successfully describes the permeation behavior of the spherulitic E/EP diblock copolymers for a wide range of compositions. The model assumes that the majority of the transport takes place along the more conductive, amorphous EP lamella but recognizes the smaller, but nonzero, permeability of the semicrystalline E domains. The observed lowering of the permeability of the copolymer by the presence of these semicrystalline E regions is accounted for in the model through considerations of its volume fraction and through an effective tortuosity. The permeabilities to He and CO<sub>2</sub> of the E/EP/E 25/50/25 specimen with the lamellae aligned in parallel ( $P_{\text{par}}$ ) and in series ( $P_{\text{ser}}$ ) with respect to the permeation direction was measured and is compared in Table 3 with the permeability values  $P_{\text{sph}}$  of the spherulitic specimen and the predictions of appropriate idealized models of permeability behavior for these three cases. Input values to the models for the pure amorphous EP and the semicrystalline E moieties have been reported previously.<sup>13</sup>

The good agreement between the various permeation models and the corresponding experiments suggests that permeabilities of semicrystalline block copolymers can be anticipated from (a) knowledge of the permeabilities of the pure materials comprising the lamellar regions of the copolymer and (b) the morphological arrangement of the lamellae within the material. The observation that  $P_{\text{ser}}(\text{exp})$  is only about 10% greater than the lower bound value of  $P_{\text{ser}}(\text{model})$  suggests that the channel die processing at  $\sigma = 2.4$  MPa produced a high degree of lamellar orientation at a macroscopic scale (our permeation specimens are circular disks of about 10 cm diameter and 0.5 mm thickness). Similarly, the

very small overprediction of  $P_{\text{par}}(\text{model})$  compared to experiment indicates that the processing at higher stresses produces a macroscopically well-ordered morphology.

## 5. Summary

It has been demonstrated by the 2D SAXS spectra that two distinct lamellar orientations can be produced when a series of semicrystalline E/EP/E block copolymers of varying E block content and 100000 g/mol total molecular weight are subjected to high levels of plane strain compression. When the E/EP/E triblocks are deformed above the E block at 150 °C using a 2.4 MPa applied stress on the channel die, the lamellae orient parallel to the plane of shear, while processing above the melt at an applied stress of 8.0 MPa, causes the lamellae to orient perpendicular to the plane of shear.

The morphology produced above the melting point for the E/EP and E/EP/E systems was attributed to the proximity of the order-disorder transition to the processing temperature. When the processing is carried out at high applied stresses, the heterogeneous melt orients perpendicular to the shear planes and then upon cooling the E block chains crystallize within the amorphous lamellar microdomains. The semicrystalline systems offer the advantage that the crystallographic texture, which is eventually locked into the materials when cooled below  $T_m$  provides an independent set of clues regarding the orientation of the lamellae at the point when crystallization takes place. The variation of the long period with molecular weight and composition is qualitatively consistent with the predictions of theory although the detailed connection between this morphological length scale and molecular level organization remains unclear.

The simple permeability model, used for the E/EP diblocks,<sup>13</sup> is in excellent agreement with the experimentally measured values for the series, spherulitic and parallel E/EP/E 25/50/25 triblock system. The permeability results and model predictions confirm the results of our SAXS experiments and indicate that almost perfect orientation of the semicrystalline lamellae can be achieved through channel die processing.

**Acknowledgment.** This research has been supported by the Office of Naval Research and the Goodyear Tire and Rubber Company.

## References and Notes

- Cohen, R. E.; Ramos, A. R. *Adv. Chem. Ser.* **1979**, *176*, 237.
- Lim, C. K.; Cohen, R. E.; Tschoegl, N. W. *Adv. Chem. Ser.* **1971**, *99*, 397.
- Caruthers, J. M.; Cohen, R. E. *Rheol. Acta* **1980**, *606*.
- Balsara, N. P.; Hammouda, B.; Kesani, P. K.; Jonnalagadda, S. V.; Straty, G. C. *Macromolecules* **1994**, *27*, 2566.
- Cates, M. E.; Milner, S. T. *Phys. Rev. Lett.* **1989**, *62*, 1856.
- Almdal, K.; Koppi, K. A.; Bates, F. S. *Macromolecules* **1992**, *25*, 1743.
- Koppi, K. A.; Tirrell, M.; Bates, F. S. *Phys. Rev. Lett.* **1993**, *70* (10), 1449.
- Koppi, K. A.; Tirrell, M.; Bates, F. S.; Almdal, K.; Colby, R. H. *J. Phys. II* **1993**, *2* (11), 1941.
- Han, C. D.; Baek, D. M.; Kim, J. K. *Macromolecules* **1990**, *23*, 561.
- Koberstein, J. T.; Russell, T. P.; Walsh, D. J.; Pottick, L. *Macromolecules* **1990**, *23*, 877.
- Kofinas, P.; Cohen, R. E. *Macromolecules* **1994**, *27*, 3002.
- Kofinas, P. Ph.D. Thesis, MIT, 1994.
- Kofinas, P.; Cohen, R. E.; Halasa, A. F. *Polymer* **1994**, *35*, 1229.
- Halasa, A. F. U.S. Patent 3 872 072.

- (15) Cohen, R. E.; Cheng, P.-L.; Douzinas, K.; Kofinas, P.; Berney, C. V. *Macromolecules* **1990**, *23*, 324.
- (16) Douzinas, K. C.; Cohen, R. E.; Halasa, A. F. *Macromolecules* **1991**, *24*, 4457.
- (17) Lin, L.; Argon, A. S. *Macromolecules* **1992**, *25*, 4011.
- (18) Song, H. H.; Argon, A. S.; Cohen, R. E. *Macromolecules* **1990**, *23*, 870.
- (19) Galeski, A.; Argon, A. S.; Cohen, R. E. *Macromolecules* **1992**, *25*, 5705.
- (20) Gray, R. W.; Young, R. J. *J. Mater. Sci.* **1974**, *9*, 521.
- (21) ASTM D-1434, American Society for Testing and Materials: Philadelphia, 1984.
- (22) Leibler, L. *Macromolecules* **1980**, *13*, 1602.
- (23) Bates, F. S.; Schultz, M. F.; Rosedale, J. H. *Macromolecules* **1992**, *25*, 5547.
- (24) DiMarzio, E. A.; Guttman, C. M.; Hoffman, J. D. *Macromolecules* **1980**, *13*, 1194.
- (25) Whitmore, M. D.; Noolandi, J. *Macromolecules* **1988**, *21*, 1482.
- (26) Rangarajan, P.; Register, R. A.; Fetter, L. J.; *Macromolecules* **1993**, *26*, 4640.
- (27) Csernica, J.; Baddour, R. F.; Cohen, R. E. *Macromolecules* **1989**, *22*, 1493.
- (28) Csernica, J.; Baddour, R. F.; Cohen, R. E. *Macromolecules* **1987**, *20*, 2468.
- (29) Csernica, J.; Baddour, R. F.; Cohen, R. E. *Macromolecules* **1990**, *23*, 1429.
- (30) Michaels, A. S.; Vieth, W. R.; Barrie, J. A. *J. Appl. Phys.* **1963**, *34* (1), 1.
- (31) Mohr, J. M.; Paul, D. R. *J. Appl. Polym. Sci.* **1991**, *42*, 1711.

MA9410328